

1 Numerical investigation of the influence of casting techniques on fiber 2 orientation distribution in ECC

3 Chung Nguyen Van ^{a,1}, Hai TranThanh ^{b,c*}, Thuc Nhu Nguyen ^b, Jianchun Li ^b

4 ^a Ho Chi Minh City University of Technology and Education, Ho Chi Minh City, Vietnam.

5 ^b School of Civil and Environmental Engineering, University of Technology Sydney, Sydney, NSW 2007,
6 Australia.

7 ^c Hue Industrial College, Hue City, Vietnam.

8 Abstract

9 Engineered cementitious composites (ECC), also known as bendable concrete, were
10 developed based on engineering the interactions between fibers and cementitious matrix. The
11 orientation of fibers, in this regard, is one of the major factors influencing the ductile behavior
12 of this material. In this study, fiber orientation distributions in ECC beams influenced by
13 different casting techniques are evaluated via numerical modeling of the casting process. Two
14 casting directions and two casting positions of the funnel outlet with beam specimens are
15 modeled using a particle-based smoothed particle hydrodynamics (SPH) method. In this SPH
16 approach, fresh mortar and fiber are discretized by separated mortar and fiber particles, which
17 smoothly interact in the computational domain of SPH. The movement of fiber particles is
18 monitored during the casting simulation. Then, the fiber orientations at different sections of
19 specimens are determined after the fresh ECC stops flowing in the formwork. The simulation
20 results show a significant impact of the casting direction on fiber orientation distributions along
21 the longitudinal wall of beams, which eventually influence the flexural strength of beams. In
22 addition, casting positions show negligible influences on the orientation distribution of fibers
23 in the short ECC beam, except under the pouring position.

24 **Keywords:** ECC; Fiber orientation distribution; Casting direction; Casting position.

25 **1. Introduction**

26 Engineered cementitious composites (ECC) are materials exhibiting high tensile ductility
27 compared to conventional concrete through optimizing the micro-mechanical interactions
28 between short-random fibers and cementitious matrix. For this reason, the matrix of ECC
29 contains only sands, cementitious materials, and no coarse aggregates [1]. These interactions
30 determine the fiber-bridging strength, which limits the crack width of ECC to normally less
31 than 60 μm [2]. The tensile strain-hardening behavior of ECC is achieved through the steady
32 formation of multiple flat cracks at different defect zones in its matrix. In other words, this
33 unique property of ECC is governed by the fiber-bridging behavior at its cracked planes [3, 4].

34 In recent decades, extensive efforts have been made to understand the influencing factors
35 on the efficiency of bridging fibers in ECC. Consequently, fiber orientation and distribution at
36 cracked planes have been recognized as the two vital factors governing fiber-bridging behavior
37 [5, 6]. Fibers should be well distributed, to ensure consistency for bearing stress at different
38 crack planes. [7]. The orientation of a fiber determines its ultimate strength when bearing stress
39 [8, 9]. The efficiency of fibers in bearing stress at a crack plane released by the matrix thus
40 strongly depends on the number of intersected fibers and their orientation at that plane [10, 11].
41 In this regard, it is desirable to improve the fiber dispersion and understand factors affecting
42 fiber orientation in ECC elements.

43 For a number of fiber-reinforced cement-based materials owning self-compacting or
44 flowable properties, experimental studies have indicated that fiber orientation might be affected
45 by formwork geometry and casting flows [12]. Different casting techniques have been
46 performed to investigate their influences on rigid steel fiber orientation distribution in beam
47 specimens [13, 14]. On the other hand, Kanakubo et al. [5] used a water glass solution to
48 simulate two casting directions of the same size of ECC specimens using flexible synthetic
49 fibers. The results of fiber orientation evaluation have illustrated the effectiveness of casting

50 directions on fibers orientation in ECC specimens. In the later work of Ding et al. [10], three
51 groups of ECC beams were cut from a slab in different directions with respect to the casting
52 direction, i.e., parallel, perpendicular and diagonal directions. The “parallel” beams attained a
53 greater degree of smaller orientation of fibers with the longitudinal direction and thus achieved
54 higher tensile stress-strain behavior than that of in “perpendicular” and “diagonal” beams. This
55 observation emphasized that understanding the influence of casting techniques on fiber
56 orientation is vitally important, especially for structural members such as beams or slabs [15,
57 16]. However, it is worth noting that observation and determination of fiber orientation in the
58 above-mentioned experimental studies required image processing and analysis procedures,
59 which are time-consuming and expensive. Moreover, in the experimental approach, the
60 variation of fiber orientation distribution in the fresh mixture at the beginning of castings might
61 also cause the dissimilarity of fiber orientations in different specimens of the hardened
62 concrete.

63 Due to the above-mentioned limitations of experimental approach, numerical models have
64 been developed to provide an alternative approach to study the flow characteristics of flowable
65 fiber reinforced cement-based materials and to investigate distribution and orientation of fibers.
66 [17-20]. In these models, fibers are typically simulated either as rigid bodies represented by
67 two-end particles for steel fibers [19, 21] or as bendable bodies represented by interconnected
68 particles for synthetic fibers [20]. The computational domains of fresh mixes are discretized
69 into sets of particles, then approximately solved using Lattice Boltzmann [22] or Smoothed
70 Particle Hydrodynamics (SPH) [17, 20] methods. The introduction of fibers into concrete
71 mixes increases the viscosity of fresh concrete. Fiber particles are simply considered as passive
72 markers, which move and orient according to the motion of fresh mixes. With this
73 consideration, Tran et al. [23] developed and validated a 3D model to simulate the flow of fresh
74 and flowable ECC. This approach has an advantage of monitoring the movement of fibers to

75 provide a practical understanding of the distribution and orientation of fibers in structural
76 elements [24]. The outcome is important in optimizing the casting technique to achieve the
77 anticipated fiber orientation for improving the material performance in ECC structural
78 elements.

79 Accordingly, the effect of casting techniques on the orientation distribution of synthetic
80 fiber in ECC beams is numerically investigated in this paper. Two casting directions (i.e.,
81 parallel and perpendicular to the longitudinal direction of the beams) and two casting positions
82 (i.e., at the middle and end of the beams) of the pouring outlet are modeled. The flow of fresh
83 and flowable ECC during the casting process is simulated by adopting the 3D SPH modeling
84 [23]. When the casting processes are completed, fiber orientations with the longitudinal
85 direction at different sections of beams are determined for comparison. Moreover, the
86 distribution of fiber orientations regarding different casting techniques is also evaluated and
87 discussed.

88 **2. Modeling of the casting process of ECC beams**

89 *2.1. Rheology model*

90 The casting of flowable ECC beam is a process of fresh materials flowing from their dropped
91 place under the funnel outlet to the other parts of formworks. This can be considered as a free-
92 surface flow of a viscous fluid. As a flowable viscous material, its flow behavior can be
93 classified as a Newtonian or non-Newtonian fluid. However, it is practical to treat flowable
94 ECC as a non-Newtonian fluid since the relationship between its shear stress and shear rate is
95 nonlinear, and its effective viscosity varies with time and rate of deformation [20, 25].
96 Moreover, the non-Newtonian fluids have yield stress, which controls the initial stage of the
97 flow. In this regard, the fluid only starts to flow once the yield stress τ_y is exceeded, and when

98 the shear stress falls below the yield stress, the fluid stops flowing. These relationships are
99 expressed in Eq. (1) and Eq. (2) as:

$$\tau = \tau_y + \mu\dot{\gamma} \quad \text{for } \tau > \tau_y \quad (1)$$

$$\mu_{eff} = \frac{\mu_0 + K\dot{\gamma}\mu_\infty}{1 + K\dot{\gamma}} \quad (2)$$

100 where μ_{eff} , μ_0 and μ_∞ are the effective viscosity, viscosity at very low and very high shear
101 strain rate $\dot{\gamma}$, respectively, and K is a constant parameter [26].

102 In the experimental approach, the plastic viscosity and yield stress of fresh cement-based
103 materials are measured using rheometers. However, different rheometers or measured times
104 provide different results of these two parameters [27, 28]. Moreover, incorporating fibers in
105 flowable concrete would make obtaining reliable values of these measurements more
106 challenging [29]. Thus, attempts to obtain accurate rheology parameters in the laboratory for
107 modeling input might not be successful. Consequently, several numerical methods have been
108 developed to estimate these two parameters for modeling fresh flowable concrete. In the
109 relevant studies, the yield stress was first assumed, and then the plastic viscosity was
110 numerically determined [29, 30]. This numerical approach was also applied to estimate its yield
111 stress and plastic viscosity for flowable ECC [20].

112 2.2. Particle-based SPH modeling

113 Due to the large deformation of flowable ECC during the casting process, the mesh-free or
114 particle-based SPH is a powerful method for solving the governing equations during ECC flow.
115 In SPH, the entire domain of fresh ECC and formwork are modeled by individual particles,
116 including mortar, fiber, and wall-boundary particles. These presented particles generate
117 interactions between mortar, fiber, and the fixed boundary. Also, the synthetic fiber is modeled

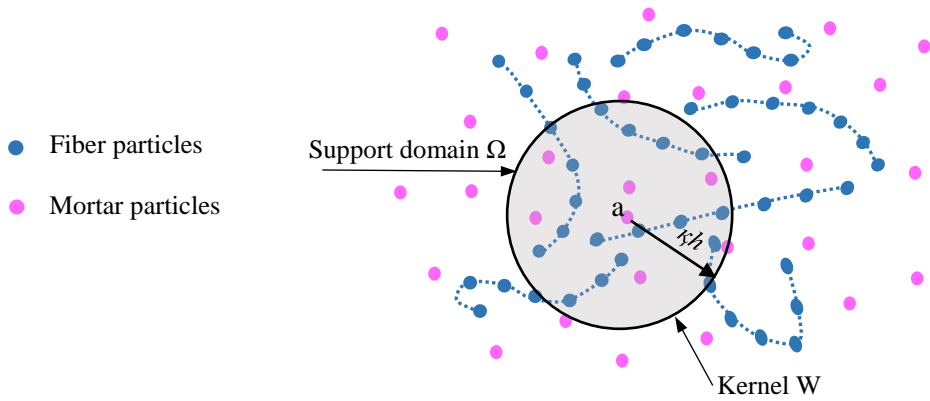
118 as inter-connected particles, and thus its two adjacent particles are considered to interact with
 119 each other during their movement.

120 The Lagrangian form of SPH allows tracking the changes in particles' properties during
 121 their interaction and motion. At each step of motion, the gradient field variables of a current
 122 particle a is approximated by a summation of all surrounding particles b in the support domain
 123 Ω of the kernel function W (Fig. 1). The governing equations of a viscous fluid can be written
 124 in the SPH forms for flowable ECC as:

$$125 \quad \frac{d\rho_a}{dt} = \sum_b m_b (\mathbf{v}_a - \mathbf{v}_b) \nabla_a W_{ab} \quad (3)$$

$$126 \quad \frac{d\mathbf{v}_a}{dt} = - \sum_b m_b \left(\frac{P_a}{\rho_a^2} + \frac{P_b}{\rho_b^2} \right) \nabla_a W_{ab} + \mathbf{g} + \sum_b m_b \left(\frac{\boldsymbol{\tau}_a}{\rho_a^2} + \frac{\boldsymbol{\tau}_b}{\rho_b^2} \right) \nabla_a W_{ab} \quad (4)$$

127 where P , ρ and t represent the pressure, particle density and time, respectively. The vector
 128 forms of the particle velocity and the gravitational acceleration are denoted by \mathbf{v} , and \mathbf{g} ,
 129 respectively.



130

131 **Fig. 1.** Fiber, mortar particles and the support domain Ω of the kernel function W .

132 As can be seen in Fig. 1, mortar and fiber particles are considered as neighboring particles,
 133 and they are included when calculating the forces acting on each other in the support domain
 134 Ω . When adding fibers into fresh mortar to produce fresh ECC, plastic viscosity increases due
 135 to the interfacial bond between fibers and fresh mortar. Therefore, the SPH method considers

136 fiber particles as passive markers and possessing the same continuum properties as mortar
137 particles. Their motions are mainly governed by the effective viscosity (Eq. 2), which
138 determines the shear stress tensor τ in Eq.4 between adjacent particles.

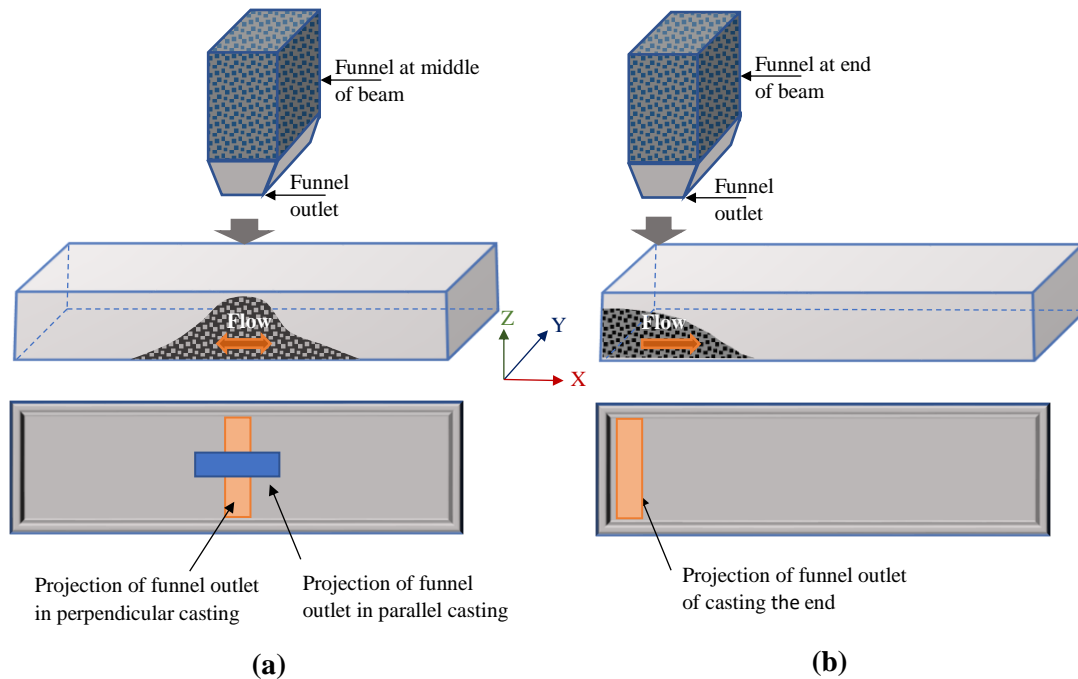
139 At each time step of the simulation, the velocity and density of mortar and fiber particles
140 are first calculated based on Eqs. 3 and 4. Then, the coordinates of a particle a in three-
141 dimensional space XYZ, i.e. $a(x, y, z)$ are updated based on its previous coordinates.
142 Subsequently, fibers' orientation distributions in a specimen are feasibly evaluated through
143 their coordinates in XYZ space when the casting simulation is completed.

144 **3. Configurations of casting techniques and fiber orientation evaluation**

145 *3.1. Initial configurations and parameters*

146 To simulate the casting process of flowable ECC, the boundary particles represented for the
147 funnel and formworks are first created. The position of the funnel outlet and its direction are
148 dependent on the considered casting techniques. Fig. 2a displays the projection of the funnel
149 outlet in the cases of parallel and perpendicular casting, in which the container of initial
150 materials is located at the middle of beams. As can be seen in Fig. 2b, the projection of the
151 funnel outlet is perpendicular to the longitudinal beam when two casting positions are studied,
152 i.e., middle-cast and end-cast beams. Then, mortar and synthetic fiber particles are created in a
153 square grid form in the funnels. The volume of container funnels is ensured to be equivalent to
154 the beams' volume. Synthetic fibers are created as straight structures with similar random
155 distribution and orientation at the beginning of the simulations. The distance between the two
156 neighboring particles within a fiber is chosen to equal 2 mm. Using 12 mm length of PVA
157 fibers, a fiber is represented by seven inter-connected particles. Moreover, fiber particles are
158 generated randomly, and their inclination with the longitudinal axis of the beam is in a range
159 of 0 to 90 degrees. The width of the funnel outlet is selected to be equal to 20 mm, which is

160 approximately 1.5 times larger than the length of fibers. This selection allows fibers to freely
 161 rotate when they flow through the funnel outlet. Additionally, the beams' formwork height is
 162 modeled higher than that of the beams to ensure particles would not spill out during their flow.



163 (a) (b)
 164 **Fig. 2.** (a) Perpendicular and Parallel casting at the middle of the beam; (b) Perpendicular casting at
 165 the end of beam.

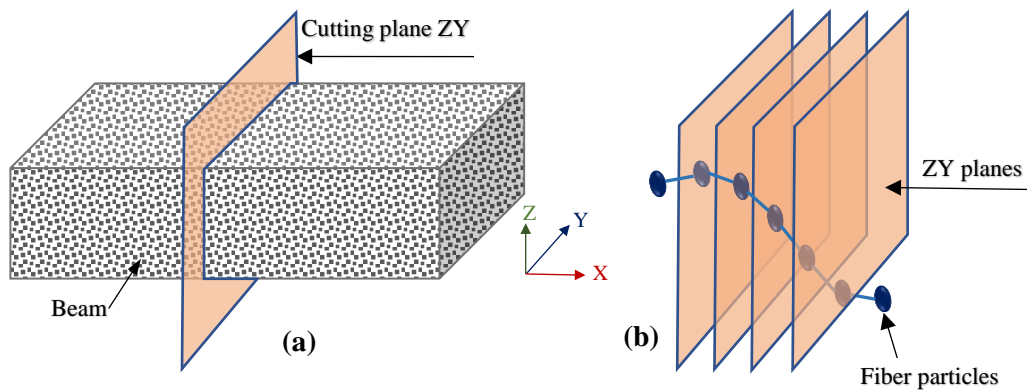
166 The material properties of ECC-M45 in Lepech and Li [31] are utilized as reference data for
 167 the simulations. The number of PVA fibers involved in the simulation is determined through
 168 its 2% volume in ECC and created mortar particles. The values of two-rheology parameters,
 169 including the yield stress $\tau_B = 165$ Pa and the plastics viscosity $\mu_B = 17$ Pa. s, are chosen as
 170 in Tran et al. [20].

171 3.2. Fiber orientation evaluation

172 The tensile strain-hardening behavior of ECC is characterized by forming multiple micro-
 173 cracks under tension. In practice, these micro-cracks are observed to be approximately
 174 perpendicular to the loading direction. Although the crack spacing depends on the stress

175 transfer from bridging fibers at crack planes, the crack spacing in ECC is typically less than 2
176 mm [32, 33]. These micro-cracks are considered to be flat and perpendicular to the loading axis
177 in the numerical approach. Thus, to evaluate the orientation of fibers at crack planes, beams
178 are virtually cut by multi-vertical planes ZY when the casting simulation of beams is
179 completed, as shown in Fig. 3a. The spacing of cutting planes are chosen to be equal to 2 mm.

180 Once synthetic fiber particles move along with mortar particles, they become bent during
181 the casting process. Through this bending phenomenon, the distance between two adjacent
182 fiber particles within a fiber when completed casting is always equal or less than their initial
183 assigned distance. Also, a fiber might intersect several cutting ZY planes with virtual lines
184 connecting its represented particles, which is illustrated in Fig. 3b. If two adjacent particles of
185 fiber are fully located between two ZY planes, they will not bridge the crack, and thus, their
186 orientation will not be determined. At a ZY plane, two inclined angles of an intersected fiber
187 regarding the XY and XZ planes are trigonometrically calculated via particles' coordinates (x ,
188 y , z).



189

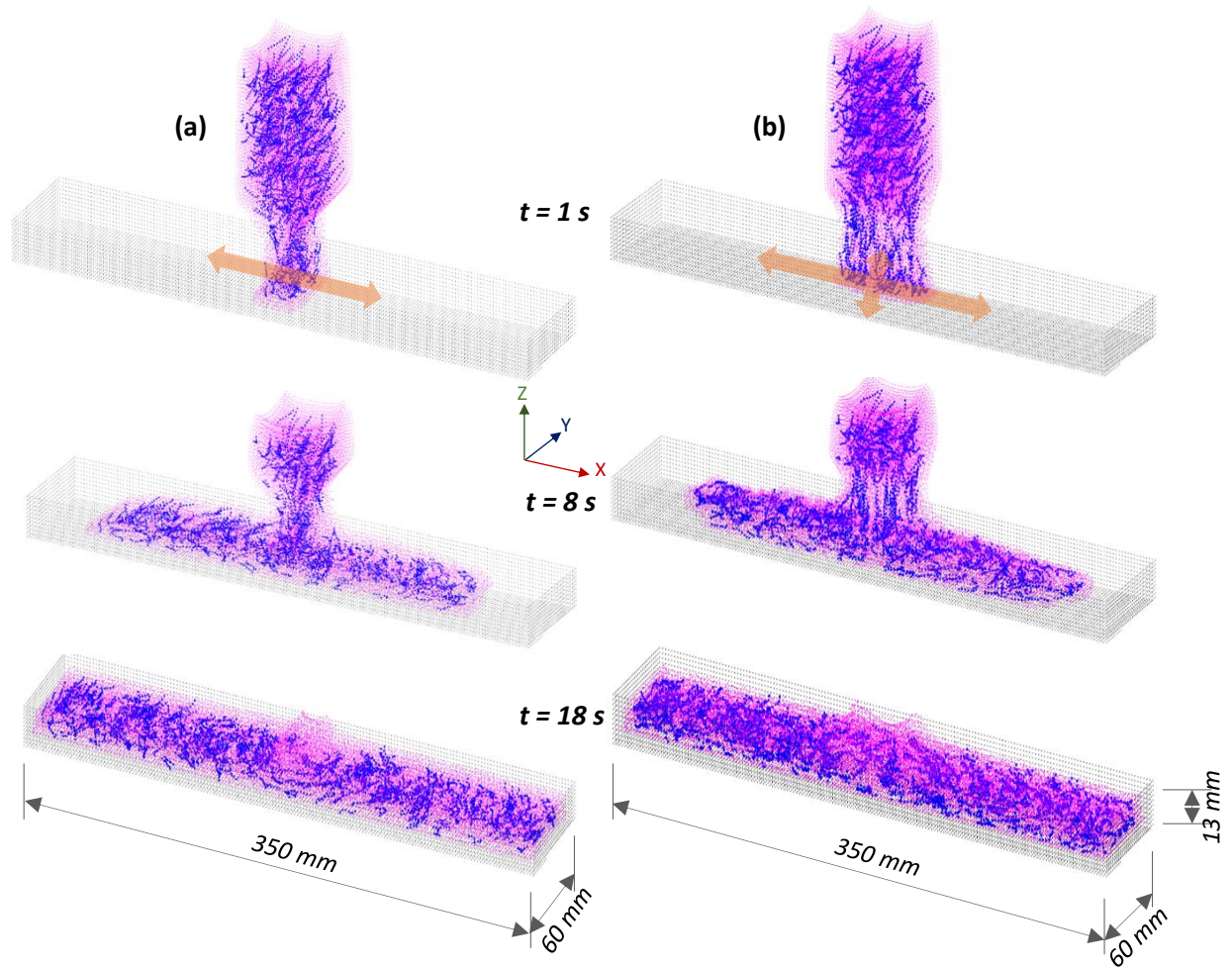
190 **Fig. 3.** (a) Cutting a beam with vertical ZY planes; (b) Fiber intersects several ZY planes

191 **4. Casting simulation, results and discussion**

192 *4.1. Perpendicular and parallel casting directions*

193 *4.1.1. Casting flow patterns*

194 In this section, two casting directions of the funnel outlet, i.e., perpendicular and parallel
195 directions relative to the longitudinal beam, are modeled. At first, 30,625 mortar particles are
196 created in the funnel with the x, y, and z axes spacing equal to 2 mm. Then, the number of
197 fibers is calculated as 2% of mortar particles (i.e., $2\% \times 30,625 = 613$ fibers), which are
198 represented by 4,291 fiber particles. These particles are generated to cast a beam of size 13 mm
199 \times 60 mm \times 350 mm from its center. Figs. 4a and 4b show the obtained flow patterns from two
200 casting directions at three-time steps. During the casting process, mortar and fiber particles
201 drop through the bottom outlet of the funnel to the bottom of the beam below the funnel
202 position, then flow to different parts of the beam. As mortar and fiber particles are assigned to
203 possess identical continuum properties, they flow smoothly together during the casting process.
204 Material particles gradually stop moving after 18 seconds, and thus the computational modeling
205 for casting simulation is stopped at this time. Additionally, it can be observed that the flow
206 speeds are relatively similar for both casting directions.



207

208 **Fig. 4.** Casting flow patterns at three-time steps $t = 1$ s, $t = 8$ s and $t = 18$ s: (a) Perpendicular casting;

209

(b) Parallel casting

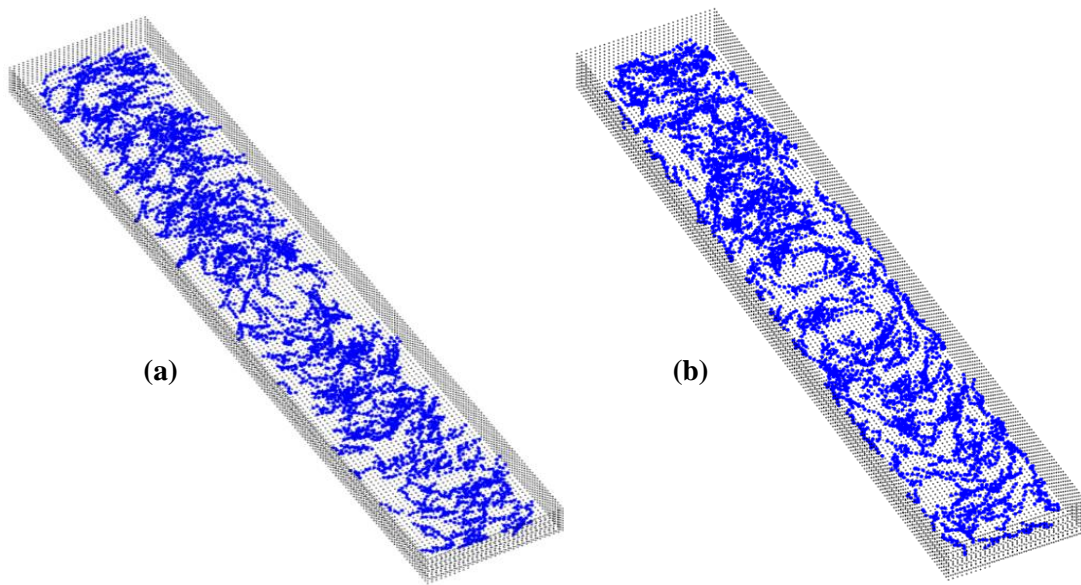
210 4.1.2. Orientation of fibers

211

212 The orientation of fibers at cutting planes ZY are quantified following the mentioned details
 213 in Section 3.2. Fig. 5a and Fig. 5b show the 3D view of fiber orientation distributions in two
 214 beams. It is observed that more fibers tend to orient parallel with the longitudinal wall in the
 215 parallel casting in comparison to the perpendicular casting. This observation can be explained
 216 by the flow of fresh ECC in the case of parallel casting pushes fibers toward the longitudinal
 217 walls of the beam more strongly than in the case of the perpendicular casting. Therefore, the
 218 inclined angles of fibers with respect to the XZ plane in the parallel casting case are lower than
 those in the perpendicular casting, as clearly seen through their polynomial fitting curves in

219 Fig. 6b. Consequently, while the inclinations of fibers relative to the XZ plane noticeably
220 distribute from around 20 degrees to 35 degrees for the parallel casting, whereas a larger
221 number of fibers orientate within the range from 35 degrees to 55 degrees in the perpendicular
222 casting (Fig. 7b).

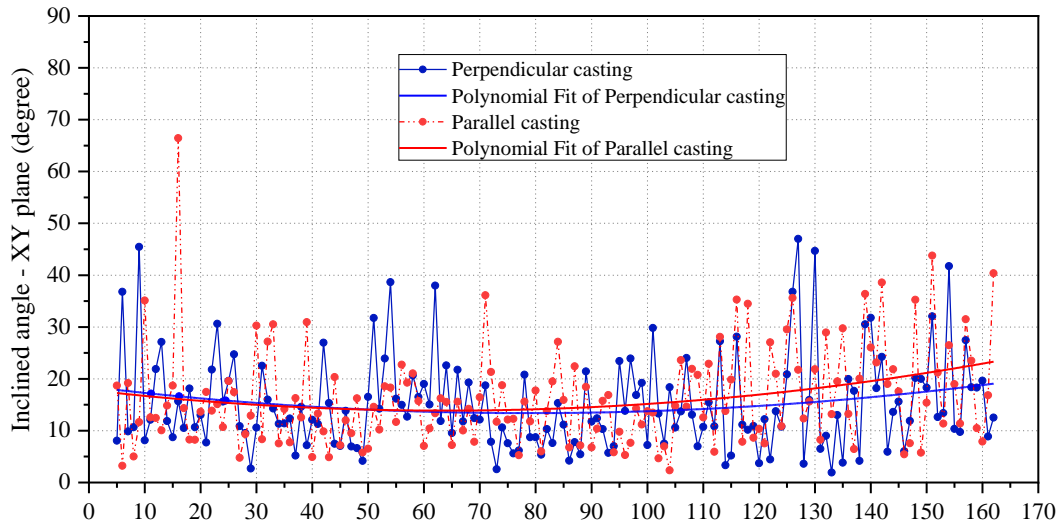
223 In addition, fibers tend to parallel with the bottom formwork, in which both casting
224 directions attain an average of fiber inclinations with the XY plane at around 15 degrees, as
225 illustrated in Fig. 6a. The reason for this small inclination value is that the 13 mm thickness of
226 the beam in this model causes the 12 mm length of fiber to become more difficult to rotate in
227 almost two-dimensional spaces during their motion. As shown in Fig. 7a, the differences in
228 fiber orientation distribution with the XY plane are insignificant for the two casting directions.



229

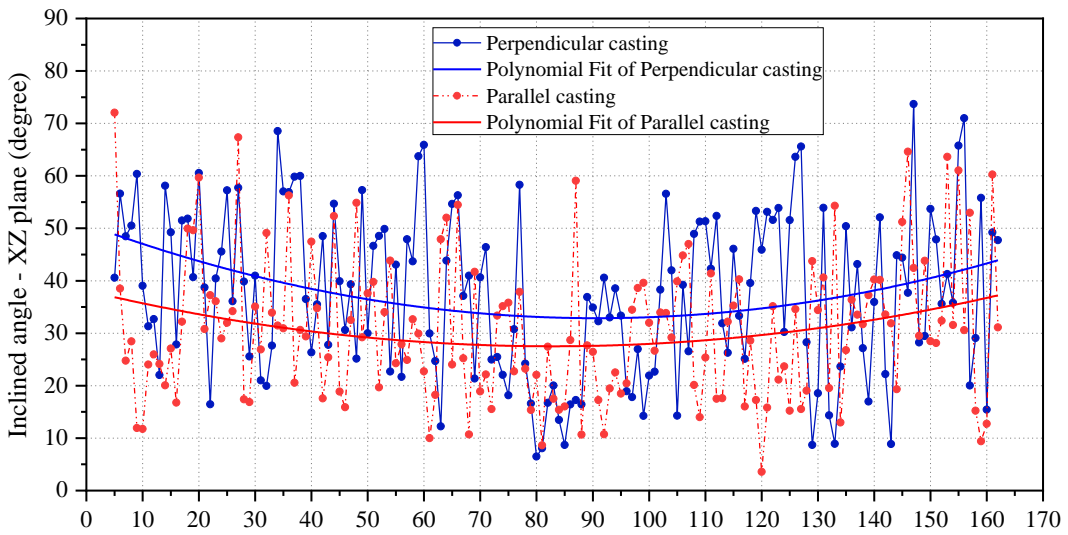
230 **Fig. 5.** The 3D view of fiber orientation distribution in beams when the casting completed: (a)

231 Perpendicular casting; (b) Parallel casting.



(a) Vertical cross sections along the beams.

232



(b) Vertical cross sections along the beams.

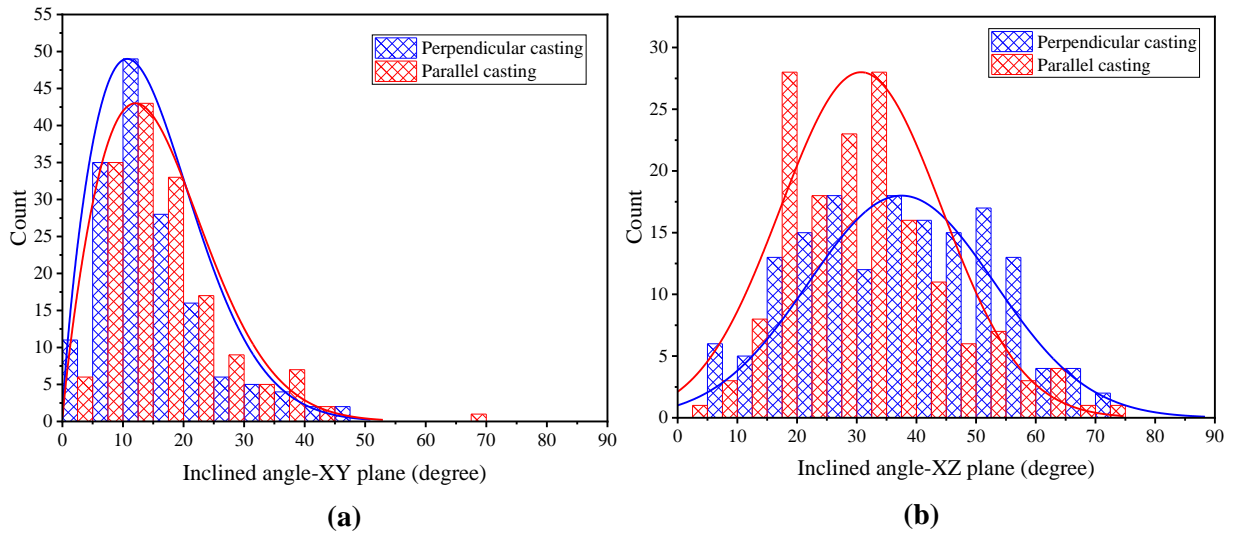
233

234

Fig. 6. Orientation of fibers at cutting planes along beams with two casting directions: (a)

235

Inclined angle of fibers with XY plane; (b) Inclined angle of fibers with XZ plane



236

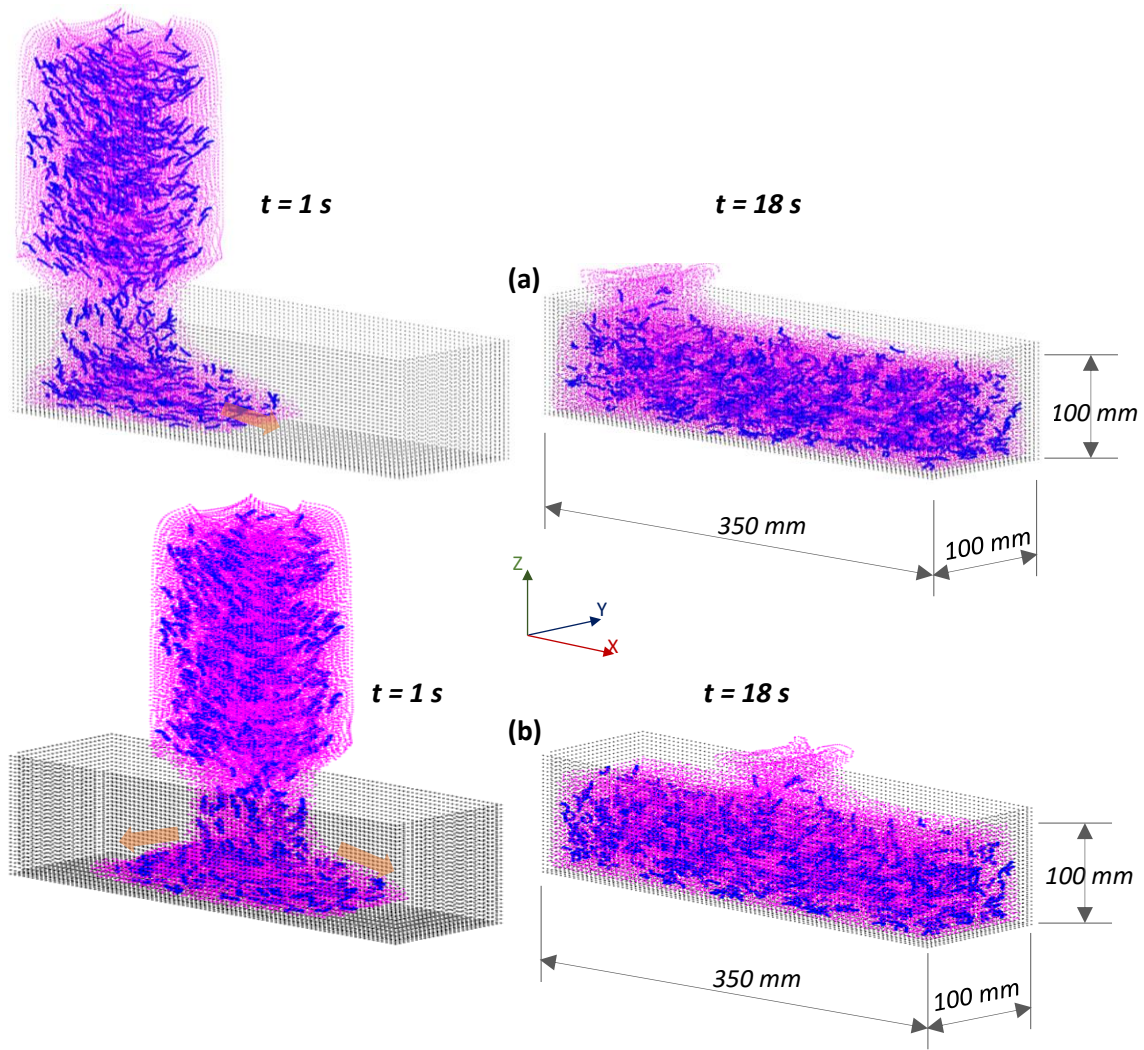
237 **Fig. 7.** Distribution of fiber orientation with two casting directions: (a) Inclined angle of fibers

238 with XY plane; (b) Inclined angle of fibers with XZ plane

239 *4.2. Casting at the end and middle of beam*

240 *4.2.1. Casting flow patterns*

241 To study the influences of casting positions on fiber orientations, two casting processes of
 242 the beam of dimensions 100 mm × 100 mm × 350 mm are simulated in which the funnel's
 243 positions are at the end and middle of beams. In these models, the thickness of beams is
 244 increased to ensure fibers can rotate freely in 3D during their flow. The initial x, y, and z axes
 245 spacing of mortar particles in the funnel is also increased to 4 mm to reduce the computational
 246 time. This size of beams requires 50,688 mortar particles and 7,098 fiber particles to represent
 247 the fresh ECC. Simulation results at two-time steps of two casting positions are illustrated in
 248 Fig. 6. Fresh materials flow from one end to another end of the beam in the case of casting at
 249 the end. For the middle-cast beam, materials flow from the center of the beam to its ends in
 250 two opposite directions.



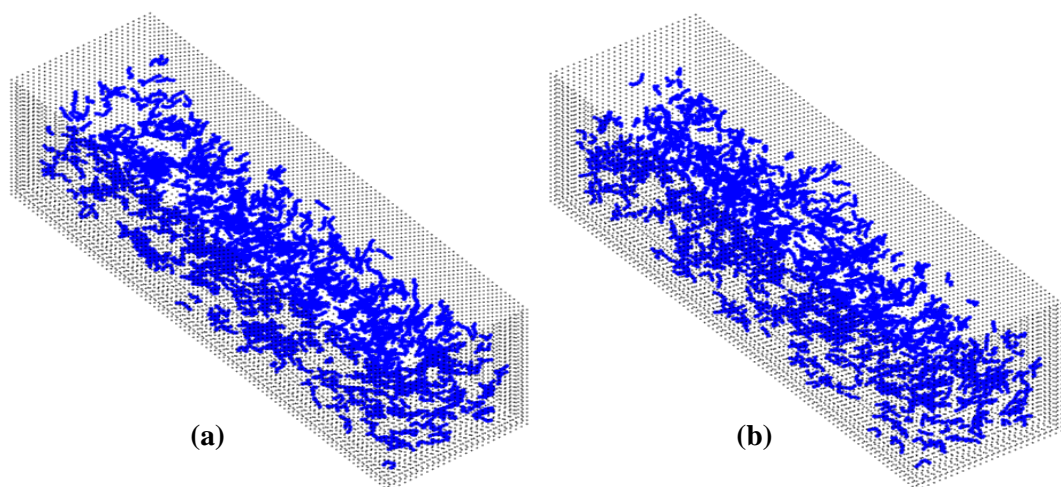
251

252

Fig. 8. Flow patterns of casting at the end of beam at two-time steps $t = 1 s$ and $t = 18 s$.

253

4.2.1. Orientation of fibers

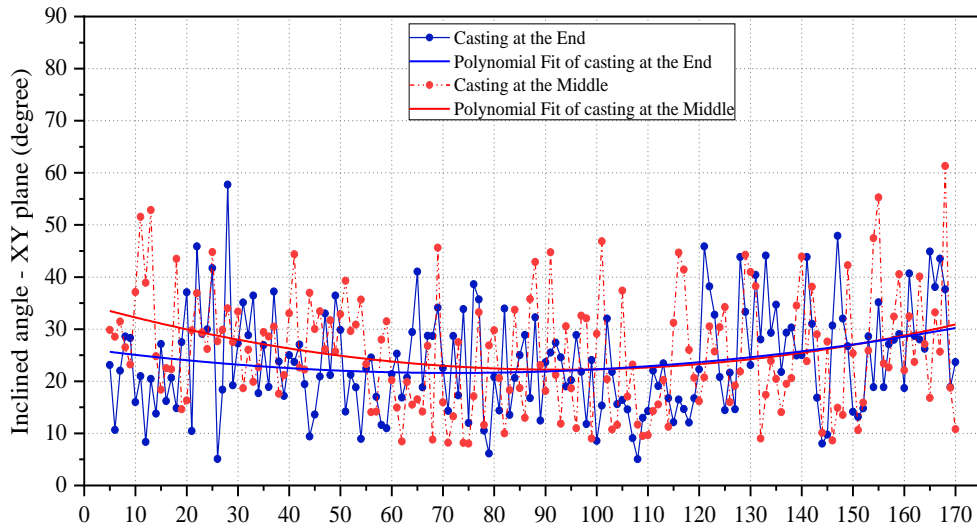


254

255 **Fig. 9.** The 3D view of fiber orientation distribution in beams when the casting is completed:
256 (a) Casting at the end of beam; (b) Casting at the middle of beam.

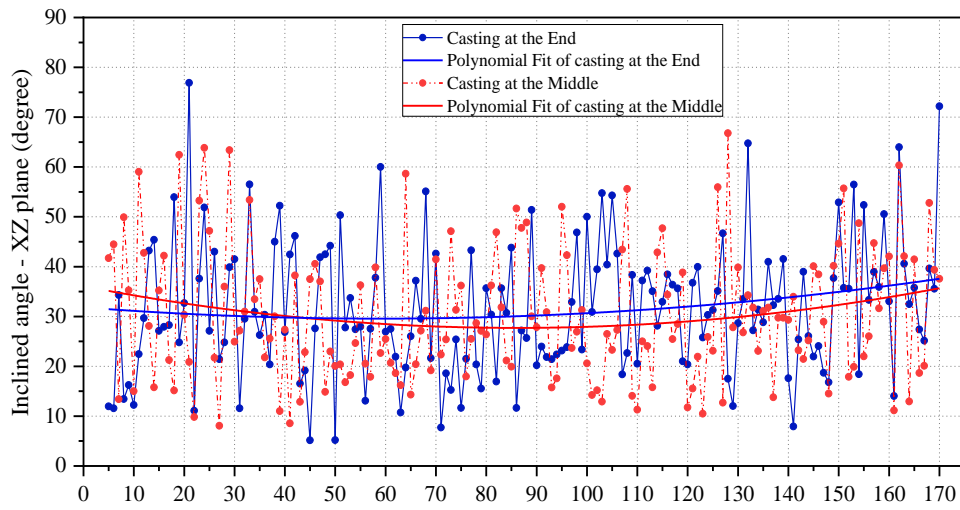
257 Fig. 9a and Fig. 9b present the 3D view of fiber orientation distribution in two beams when
258 the simulations are completed. It is hard to visually recognize any differences in fiber
259 orientation distribution in two beams of two casting positions from these two figures. For a
260 quantitative assessment, the inclined angles of fibers with XY and XZ planes for both beams
261 are also determined using the procedure mentioned in section 3.2. As plotted in Fig. 10a, fibers
262 tend to be parallel with the bottom XY plane under the funnel outlet in the end-cast beam (from
263 vertical cross-section 0 to section 40). By contrast, this phenomenon cannot be observed when
264 casting at the middle of the beam. For this reason, the number of fibers inclined with the XY
265 plane in the range of 5 degrees to 25 degrees of the end-cast beam is more than that in the case
266 of the middle-cast beam (Fig. 11a).

267 As shown in Fig. 10b, the inclination of fiber with the XZ plane in the middle-cast beam is
268 slightly lower than that of the end-cast beam, except under its funnel outlet area. When casting
269 at the middle, the flow tends to drive fiber toward the two longitudinal walls of the beam more
270 strongly than when casting at the end. As a result, the orientation distribution of fiber with the
271 XZ plane in the middle-cast beam, ranging from 25 degrees to 60 degrees, is slightly lower
272 than that in the end-cast beam (Fig. 11b). However, the size of the beam might affect the
273 gradient of the flow velocity of different casting positions, which would then influence the flow
274 to induce fiber orientation. Due to the beam dimensions used in these two simulations being
275 narrow and short, the difference in flow velocity might not be noticeable. Therefore, the
276 changes of fiber orientation distributions are negligible, except underneath the pouring position
277 of fresh materials at the funnel outlet.



278

(a) Vertical cross sections along the beams.



279

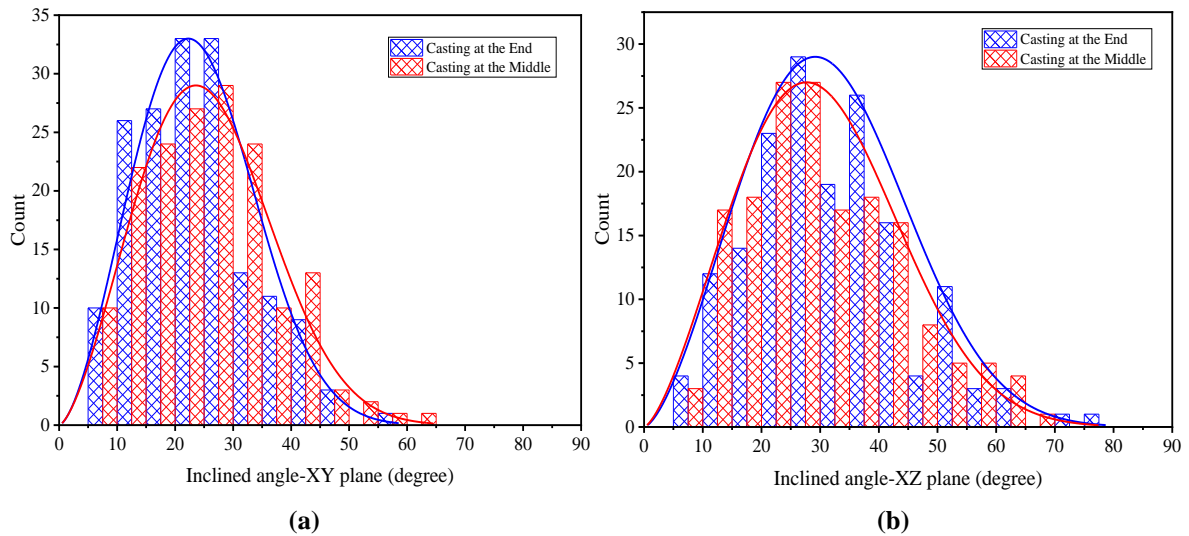
(b) Vertical cross sections along the beams

280

Fig. 10. Orientation of fibers at cutting planes along beams with two casting positions: (a)

281

Inclined angle of fibers with XY plane; (b) Inclined angle of fibers with XZ plane.



282

283

Fig. 11. Distribution of fiber orientation with two casting positions: (a) Inclined angle of fibers

284

with XY plane; (b) Inclined angle of fibers with XZ plane

285 *4.3. Discussion on the fiber orientation distribution and the flexural performance of beams*

286

It is worth mentioning that some other factors might influence the fiber orientation distribution in specimens, such as the manufacturing process or the volume of fibers. First, an inappropriate process to produce fresh ECC could lead to poor dispersion of fibers, which could eventually negatively affect fiber orientation distribution and reduce the efficiency of implemented casting techniques. Therefore, fiber dispersion needs to be controlled throughout the mixing process. It has been shown that adjusting the mixing sequence [34] and rheology control of mortar paste before adding fibers [7] are efficient to achieve better fiber dispersion. Moreover, fiber orientation distribution in beams is expected to vary when the volume/number of fibers is changed. From the experimental point of view, it is impossible to study this variation in the laboratory when changing the volume/number of fibers. In this regard, the numerical simulation in this study is an ideal method to investigate this concern, and it should be conducted in future works.

297

298 On the impact of fiber orientation, Ding et al. [10] indicated a significant increase of the
299 ultimate flexural strength and mid-span deflection of beam specimens owning smaller fiber
300 orientation distribution. This experimental result is explained by the increase in bridging stress
301 and complementary energy of smaller inclined fibers when bridging cracks. It is important to
302 note that smaller fiber orientation distribution herein indicates more fibers parallel to the
303 longitudinal direction of the beam, or more fibers perpendicular to flexural cracks. By
304 implementing different casting directions, the authors also suggested that the casting direction
305 should be parallel to the loading direction, which maximizes the bridging efficiency of fibers.
306 In this regard, with more fibers that tend to be parallel to the longitudinal walls of the beam,
307 the parallel casting beam in Section 4.1 achieves higher flexural strength as it owns lower fiber
308 orientation distribution.

309 However, the fiber orientation distribution might vary depending on the size of beams and
310 the width of the funnel outlets. On the one hand, fiber orientations might be redistributed when
311 they flow through a narrow funnel outlet. In this regard, fibers can be re-orientated in the
312 anticipated direction by adjusting the size of the outlet. On the other hand, different size of
313 beams cast by flowable fiber reinforced concrete influence their flexural performance [35, 36].
314 Picazo et al. [36] showed that small beams, which exhibited better fiber orientation distribution,
315 achieved higher flexural strength than larger beams. In this current study, the beam 13 mm ×
316 60 mm × 330 mm exhibit the average angle of fiber with XY plane is about 15 degrees (Fig.
317 6a), compared to that of around 25 degrees of the 100 mm × 100 mm × 350 mm beam (Fig.
318 10a). This result demonstrates the wall-effect on the rotation of fiber during the casting flow.
319 In small and narrow beams, a larger fiber proportion is restricted in free rotation near the wall
320 boundaries, leading to more fibers parallel with the walls. These fibers contribute to the
321 increase of the flexural strength of small beams compared to larger beams. However, it can be

322 noticed that the flow that induces fiber orientation when casting at different positions has a
323 negligible impact on the fiber orientation distribution of short beams (Fig.10).

324 **5. Conclusions**

325 The present study numerically evaluates the orientation of fibers in ECC beams considering
326 different casting techniques. Fiber orientations at different cross-sections of beams are
327 observed and evaluated by simulating the casting process of flowable ECC. The results of fiber
328 orientation evaluation considering two casting directions and two casting positions can be
329 presented as follows:

- 330 a) The direction of the funnel outlet with the longitudinal beam significantly influences
331 fiber orientation. Fibers tend to be less inclined with the longitudinal walls of beams in
332 the case of parallel casting than in the case of perpendicular casting. Thus, parallel
333 casting in which the funnel outlet parallels with the longitudinal wall of beams is
334 suggested to be implemented to increase the efficiency of fiber in bearing cracks and
335 improving the flexural strength of beams.
- 336 b) Fibers have a tendency to become parallel with the bottom of thin beams, regardless of
337 the casting directions. Moreover, thin beam tends to have a smaller fiber inclination with
338 the bottom plane than thick beams.
- 339 c) With the short beams in this study, casting positions only slightly affect the fibers'
340 orientation, except for a significantly smaller orientation of fibers with the bottom plane
341 beneath the pouring position when casting at the end of the beam.

342 Although the obtained results of fiber orientation distribution in this study agree reasonably
343 well with the findings of experimental studies in the literature, future experiments on flowable
344 ECC using synthetic fibers are desirable. The flow-induced fiber orientation might be more
345 significant for longer beams when considering different casting techniques. The flow velocity

346 gradient is also affected by the fresh-state properties of ECC materials. Therefore, different
347 fresh-state properties and longer beams are the two factors that need to be considered in future
348 studies.

349 **Acknowledgments**

350 This work belongs to the project grant T2021-97TD in 2021 funded by Ho Chi Minh City
351 University of Technology and Education, Vietnam.

352

353 **References**

- 354 1. Li, V.C., *On engineered cementitious composites (ECC)*. Journal of Advanced
355 Concrete Technology, 2003. **1**(3): p. 215-230.
- 356 2. Li, V.C., *Tailoring ECC for special attributes: A review*. International Journal of
357 Concrete Structures and Materials, 2012. **6**(3): p. 135-144.
- 358 3. Li, V.C., C. Wu, S. Wang, A. Ogawa, T. Saito, *Interface tailoring for strain-hardening*
359 *polyvinyl alcohol-engineered cementitious composite (PVA-ECC)*. Materials Journal,
360 2002. **99**(5): p. 463-472.
- 361 4. Yang, E.-H., S. Wang, Y. Yang, V.C. Li, *Fiber-bridging constitutive law of engineered*
362 *cementitious composites*. Journal of Advanced Concrete Technology, 2008. **6**(1): p.
363 181-193.
- 364 5. Kanakubo, T., M. Miyaguchi, K. Asano, *Influence of fiber orientation on bridging*
365 *performance of polyvinyl alcohol fiber-reinforced cementitious composite*. ACI
366 Materials Journal, 2016. **113**(2).
- 367 6. Ranade, R., M. Stults, B. Lee, V. Li, *Effects of fiber dispersion and flaw size*
368 *distribution on the composite properties of PVA-ECC*, in *High Performance Fiber*
369 *Reinforced Cement Composites 6*. 2012, Springer. p. 107-114.
- 370 7. Li, M.,V.C. Li, *Rheology, fiber dispersion, and robust properties of engineered*
371 *cementitious composites*. Materials and Structures, 2013. **46**(3): p. 405-420.
- 372 8. Ouyang, C., A. Pacios, S. Shah, *Pullout of inclined fibers from cementitious matrix*.
373 Journal of Engineering Mechanics, 1994. **120**(12): p. 2641-2659.
- 374 9. Leung, C.K.,N. Ybanez, *Pullout of inclined flexible fiber in cementitious composite*.
375 Journal of Engineering Mechanics, 1997. **123**(3): p. 239-246.
- 376 10. Ding, C., L. Guo, B. Chen, *Orientation distribution of polyvinyl alcohol fibers and its*
377 *influence on bridging capacity and mechanical performances for high ductility*
378 *cementitious composites*. Construction and Building Materials, 2020. **247**: p. 118491.
- 379 11. Lu, C.,C.K. Leung, *Theoretical evaluation of fiber orientation and its effects on*
380 *mechanical properties in Engineered Cementitious Composites (ECC) with various*
381 *thicknesses*. Cement and Concrete Research, 2017. **95**: p. 240-246.

- 382 12. Zhou, B.,Y. Uchida, *Influence of flowability, casting time and formwork geometry on*
383 *fiber orientation and mechanical properties of UHPFRC*. Cement and Concrete
384 Research, 2017. **95**: p. 164-177.
- 385 13. Ferrara, L., N. Ozyurt, M. Di Prisco, *High mechanical performance of fibre reinforced*
386 *cementitious composites: the role of “casting-flow induced” fibre orientation*.
387 Materials and Structures, 2011. **44**(1): p. 109-128.
- 388 14. Huang, H., A. Su, X. Gao, Y. Yang, *Influence of formwork wall effect on fiber*
389 *orientation of UHPC with two casting methods*. Construction and Building Materials,
390 2019. **215**: p. 310-320.
- 391 15. Qiao, Z., Z. Pan, W. Xue, S. Meng, *Experimental study on flexural behavior of ECC/RC*
392 *composite beams with U-shaped ECC permanent formwork*. Frontiers of Structural and
393 Civil Engineering, 2019. **13**(5): p. 1271-1287.
- 394 16. Abbas, A.A., F.H. Arna’Ot, S.R. Abid, M. Özakça, *Flexural behavior of ECC hollow*
395 *beams incorporating different synthetic fibers*. Frontiers of Structural and Civil
396 Engineering, 2021. **15**(2): p. 399-411.
- 397 17. Deeb, R., B. Karihaloo, S. Kulasegaram, *Reorientation of short steel fibres during the*
398 *flow of self-compacting concrete mix and determination of the fibre orientation factor*.
399 Cement and Concrete research, 2014. **56**: p. 112-120.
- 400 18. Huang, H., X. Gao, Y. Li, A. Su, *SPH simulation and experimental investigation of*
401 *fiber orientation in UHPC beams with different placements*. Construction and Building
402 Materials, 2020. **233**: p. 117372.
- 403 19. Bi, J., C. Bao, D. Xu, J. Guan, W. Cheng, *Numerical simulation of the distribution and*
404 *orientation of steel fibres in the SCC*. Magazine of Concrete Research, 2017: p. 1-12.
- 405 20. Tran, H., J. Li, Y. Zhang, *Numerical modelling of the flow of self-consolidating*
406 *engineered cementitious composites using smoothed particle hydrodynamics*.
407 Construction and Building Materials, 2019. **211**: p. 109-119.
- 408 21. Deeb, R., S. Kulasegaram, B.L. Karihaloo, *3D modelling of the flow of self-compacting*
409 *concrete with or without steel fibres. Part II: L-box test and the assessment of fibre*
410 *reorientation during the flow*. Computational Particle Mechanics, 2014. **1**(4): p. 391-
411 408.

- 412 22. Švec, O., J. Skoček, H. Stang, M.R. Geiker, N. Roussel, *Free surface flow of a*
413 *suspension of rigid particles in a non-Newtonian fluid: A lattice Boltzmann approach.*
414 *Journal of Non-Newtonian Fluid Mechanics*, 2012. **179**: p. 32-42.
- 415 23. Tran, H.T., J. Li, Y.X. Zhang, *Numerical simulation of self-consolidating engineered*
416 *cementitious composite flow with the V-funnel and U-box.* *Construction and Building*
417 *Materials*, 2020. **236**: p. 117467.
- 418 24. Tran, H.T., J. Li, Y. Zhang. *Numerical evaluation the effect of specimen thickness on*
419 *fibre orientation in self-consolidating engineered cementitious composites.* in *RILEM-*
420 *fib International Symposium on Fibre Reinforced Concrete.* 2020. Springer.
- 421 25. Kulasegaram, S.,B.L. Karihaloo, *Fibre-reinforced, self-compacting concrete flow*
422 *modelled by smooth particle hydrodynamics.* *Proceedings of the Institution of Civil*
423 *Engineers-Engineering and Computational Mechanics*, 2013. **166**(1): p. 22-31.
- 424 26. Shao, S.,E.Y.M. Lo, *Incompressible SPH method for simulating Newtonian and non-*
425 *Newtonian flows with a free surface.* *Advances in Water Resources*, 2003. **26**(7): p.
426 787-800.
- 427 27. Ferrara, L., M. Cremonesi, N. Tregger, A. Frangi, S.P. Shah, *On the identification of*
428 *rheological properties of cement suspensions: Rheometry, computational fluid*
429 *dynamics modeling and field test measurements.* *Cement and Concrete Research*, 2012.
430 **42**(8): p. 1134-1146.
- 431 28. Kostrzanowska-Siedlarz, A.,J. Gołaszewski, *Rheological properties of high*
432 *performance self-compacting concrete: Effects of composition and time.* *Construction*
433 *and Building Materials*, 2016. **115**: p. 705-715.
- 434 29. Ghanbari, A.,B.L. Karihaloo, *Prediction of the plastic viscosity of self-compacting steel*
435 *fibre reinforced concrete.* *Cement and Concrete Research*, 2009. **39**(12): p. 1209-1216.
- 436 30. Lashkarbolouk, H., A.M. Halabian, M.R. Chamani, *Simulation of concrete flow in V-*
437 *funnel test and the proper range of viscosity and yield stress for SCC.* *Materials and*
438 *Structures*, 2014. **47**(10): p. 1729-1743.
- 439 31. Lepech, M.D.,V.C. Li, *Large-scale processing of engineered cementitious composites.*
440 *ACI Materials Journal*, 2008. **105**(4): p. 358-366.

- 441 32. Wang, S.,V.C. Li. *Polyvinyl alcohol fiber reinforced engineered cementitious*
442 *composites: material design and performances*. in *Proc., Int'l Workshop on HFRCC*
443 *Structural Applications, Hawaii*. 2005. Citeseer.
- 444 33. Şahmaran, M.,V.C. Li, *Durability properties of micro-cracked ECC containing high*
445 *volumes fly ash*. *Cement and Concrete Research*, 2009. **39**(11): p. 1033-1043.
- 446 34. Zhou, J., S. Qian, G. Ye, O. Copuroglu, K. van Breugel, V.C. Li, *Improved fiber*
447 *distribution and mechanical properties of engineered cementitious composites by*
448 *adjusting the mixing sequence*. *Cement and Concrete Composites*, 2012. **34**(3): p. 342-
449 348.
- 450 35. Nguyen, D.L., D.J. Kim, G.S. Ryu, K.T. Koh, *Size effect on flexural behavior of ultra-*
451 *high-performance hybrid fiber-reinforced concrete*. *Composites Part B: Engineering*,
452 2013. **45**(1): p. 1104-1116.
- 453 36. Picazo, Á., M.G. Alberti, J.C. Gálvez, A. Enfedaque, A.C. Vega, *The Size Effect on*
454 *Flexural Fracture of Polyolefin Fibre Reinforced Concrete*. *Appl Sci-Basel*, 2019. **9**:
455 p. 1762.
- 456